THE ASTROPHYSICAL JOURNAL, 398:544–551, 1992 October 20

^{13}CO AND HCO$^+$ OBSERVATIONS OF *IRAS* SOURCES IN L1641

HUA CHEN
Institute for Astronomy, University of Hawaii, 2680 Woodlawn Drive, Honolulu, HI 96822
AND
YASUO FUKUI AND JI YANG[1]
Department of Astrophysics, Nagoya University, Chikusa-ku, Nagoya 464, Japan
Received 1992 January 13; accepted 1992 April 21

ABSTRACT

Twenty-eight *IRAS* sources selected from the *Infrared Astronomical Satellite* (*IRAS*) co-added images in L1641 were observed in the ^{13}CO (J = 1–0) and HCO$^+$(J = 1–0) using the 45 m telescope at the Nobeyama Radio Observatory. The ^{13}CO and HCO$^+$ column densities toward the *IRAS* sources correlated with each other, and both column densities also correlated with the *IRAS* color defined by the 12–25 μm flux ratio. Three outflow sources mapped in this study showed well-defined HCO$^+$ cores with a size of 0.1 pc and a mass of 3–30 $M_\odot$. The most probable explanation of these results is that the molecular dense cores are dissipated by both accretion and outflow during an early stage of stellar evolution.

Subject headings: infrared: interstellar: lines — ISM: individual (L1641) — ISM: jets and outflows — ISM: molecules

1. INTRODUCTION

Observational and theoretical studies have shown that young stellar objects are being formed in dense cores in molecular clouds (Myers & Benson 1983; Beichman et al. 1986; Shu, Adams, & Lizano 1987). A natural outcome is that the evolution of a young stellar object (YSO) will disperse the molecular dense core in which it forms. Protostellar objects should be deeply embedded in the cores, while more evolved stars should have dissipated the cores. This makes it of interest to study the molecular gas near to YSOs.

In molecular dense cores, CO J = 1–0 is optically thick and is usually not a good tracer of molecular column density. The optical depth of the ^{13}CO J = 1–0 transition is much smaller than the CO line, but the gas density required to excite the line emission is only 10^{2-3} cm^{-3}. For such densities, the foreground and background emission in the line of sight cannot be easily eliminated. The HCO$^+$ J = 1–0 transition is a better probe of dense molecular gas. The molecule has a much larger dipole moment, so its collisional excitation requires much higher gas densities (10^{4-5} cm^{-3}) even if the photon trapping is taken into account. In addition, the line is strong enough in the nearby molecular clouds to yield reliable detection.

The study reported here is part of a comprehensive study of YSOs in the nearby giant molecular cloud L1641. It involves *IRAS* data analysis, near-IR imaging and millimeter molecular line observations, both at a moderate angular resolution of 3′ and at a high angular resolution of 20″. In this paper we report ^{13}CO and HCO$^+$ observations of 28 *IRAS* sources selected from the *IRAS* co-added images in L1641. The sample selection and observations are explained in § 2. In § 3, we will present the observational results. We will also analyze the correlations between the molecular and the *IRAS* properties of the sources. In § 4, we will discuss the implications of the results. Major conclusions are summarized in § 5.

2. OBSERVATIONS

2.1. *Sample Selection*

L1641 is located in the southern part of the Orion Nebula at a distance of 460 pc (Cohen & Kuki 1979). Extensive studies have shown active low-mass star formation in the region. The Nagoya unbiased CO survey (Fukui et al. 1986; Fukui 1989) discovered eight CO outflows in this region, and a ^{13}CO survey of L1641 (Bally et al. 1987) found it to be very filamentary. A recent survey (Morgan et al. 1991) found several new candidates for CO outflows. Strom et al. (1989b) studied 123 sources in the *IRAS* Point Source Catalog (Version 2, 1988, hereafter PSC) that were in the L1641 region. Many of them have a flat or rising spectral energy distribution and are probably YSOs. The variety of YSOs in L1641 makes the cloud suitable for a comparative study.

To obtain a more complete sample of the YSOs in L1641, a sample of 230 sources was selected from the *IRAS* co-added images in L1641 in an unbiased manner. The source fluxes in the four *IRAS* bands were determined using the *IRAS* addscan data from the Infrared Processing and Analysis Center (IPAC). Because both the images and the addscans combine several single *IRAS* scans into a co-added scan, the sensitivity was enhanced by a factor of 2–3 over that of the PSC. To obtain the source luminosity, we used the method suggested by Emerson (1988) to integrate all the observed *IRAS* fluxes. A blackbody extrapolation was used to account for the luminosity beyond the *IRAS* detection. The details of the *IRAS* source sample will be presented in a separate paper (Chen, Tokunaga, & Fukui 1992c).

For this study, we selected 28 sources from the sample of 230 *IRAS* sources in the L1641 region. The selection was not intended to be statistically complete; the choice of sources was made to achieve a broad range of the *IRAS* colors and *IRAS* luminosities to search for correlation with dense molecular gases. In the sample, eight sources are associated with the CO outflow detected in the Nagoya survey. Sources 18 and 50 are associated with the candidates for CO outflow detected by Morgan et al. (1991). For simplicity, these 10 sources will be

[1] Postal address: Purple Mountain Observatory, Academica Sinica, Nanjing 210008, China.

TABLE 1

IRAS DATA OF THE SOURCES

Number (1)	SN (2)	α(1950) (3)	δ(1950) (4)	*f*12 (Jy) (5)	*f*25 (Jy) (6)	*f*60 (Jy) (7)	*f*100 (Jy) (8)	*L* ($L_\odot$) (9)	log (*f*12/*f*25) (10)	ID (11)	Outflow (12)	Reference (13)
3.........	3	$5^h39^m38^s$	−6°20′ 7″	0.28 U	0.32 U	2.3 U	23.8 D	6.0	...			
7.........	4	5 34 31	−6 23 22	0.38 U	0.65 E	4.8 F	29.2 F	9.4	−0.23			
8.........	6	5 33 56	−6 24 7	1.08 D	21.90 A	213.4 A	601.2 A	238.5	−1.31	L1641-N	Y	1
18.........	11	5 33 58	−6 26 37	0.70 D	3.00 D	15.0 C	65.2 U	8.0	−0.63	MB 8	Y	2
25.........	12	5 33 3	−6 28 37	1.15 A	8.60 A	36.0 A	100.7 A	44.3	−0.87	V801 Ori		3
31.........	16	5 34 37	−6 35 7	1.07 B	1.07 B	3.3 F	22.3 U	4.0	0.00	BE Ori		3
33.........	18	5 34 52	−6 36 37	1.06 C	1.07 D	7.0 F	46.6 C	16.4	0.00	BF Ori		3
34.........	19	5 33 16	−6 37 37	0.35 F	0.35 F	6.9 D	14.2 F	6.7	0.00			
37.........	23	5 34 4	−6 40 37	5.87 A	8.12 A	13.2 E	115.0 U	20.7	−0.14			
42.........	26	5 34 27	−6 43 22	0.48 U	0.86 F	7.6 E	54.2 B	16.8	−0.26			
47.........	28	5 33 58	−6 44 37	8.58 B	7.35 C	27.0 C	100.0 F	51.7	0.07	V380 Ori	Y	3
49.........	30	5 33 30	−6 45 7	0.96 B	1.94 B	29.7 A	154.9 B	51.9	−0.31			
50.........	31	5 33 58	−6 46 22	1.80 C	6.00 D	60.0 B	280.0 B	97.4	−0.52	HH 182	Y	2
51.........	32	5 33 56	−6 47 7	0.70 D	5.00 E	80.7 C	261.5 A	97.5	−0.85			3
56.........	33	5 35 24	−6 48 52	0.23 U	0.59 C	4.1 U	8.7 U	0.6	−0.42			
62.........	34	5 35 41	−6 50 52	2.82 A	3.11 A	7.1 B	55.9 A	22.6	−0.04			
68.........		5 34 38	−6 55 45	1.70 A	2.37 A	7.4 D	14.0 U	7.9	−0.14			
71.........	35	5 35 29	−6 58 22	0.15 U	0.51 C	5.3 C	26.1 U	3.2	−0.54	T546		3
73.........	36	5 36 16	−6 59 52	2.14 B	5.31 A	20.5 A	44.7 B	24.5	−0.39			
75.........	39	5 36 21	−7 2 22	0.57 C	5.34 A	26.1 A	106.5 A	39.7	−0.97	L1641-C	Y	1
79.........	40	5 35 53	−7 3 52	53.74 A	124.6 A	168.8 A	127.0 A	241.0	−0.37	Haro-13a		3
96.........		5 36 8	−7 18 22	0.89 B	1.42 A	8.3 B	23.4 C	10.9	−0.20			
104.........	54	5 36 56	−7 28 7	0.89 B	4.62 A	68.1 A	122.9 B	58.2	−0.72	H4-255	Y	1
105.........	55	5 38 2	−7 28 52	29.59 A	88.46 A	182.3 A	219.2 A	211.9	−0.48	L1641-S	Y	1
108.........	59	5 37 27	−7 31 37	0.18 U	8.99 A	128.6 A	219.9 A	104.3	−1.70	L1641-S3	Y	1
119.........	62	5 38 4	−7 38 52	0.20 U	0.78 B	2.0 D	11.0 U	1.5	−0.59			
194.........	85	5 38 27	−8 8 7	0.30 U	1.62 B	19.0 A	37.3 B	16.8	−0.73	L1641-S4	Y	1
216.........	93	5 40 22	−8 18 22	0.94 B	4.41 A	15.1 B	50.0 F	21.0	−0.67	L1641-S2	Y	1

NOTES.—Col. (1) gives the *IRAS* source number. Col. (2) is the source number assigned by Strom et al. 1989b. Cols. (3)–(4) give the coordinates of the sources (in 1950 epoch). Cols. (5)–(8) are the *IRAS* fluxes as determined by the addscan process at IPAC, and the letters following the fluxes indicate the flux uncertainty in the same way of the PSC: A, <4%; B, 4–8%; C, 8–12%; D, 12–16%; E, 16–20%; F, >20%; U denotes a 3 σ upper limit. Cols. (9)–(10) are the source luminosity and the 12–25 μm flux ratio, respectively. Col. (11) gives the source identifications. Col. (12) indicates whether the source is associated with a CO outflow. Col. (13) gives the references as follows: (1) Fukui 1989); (2) Morgan et al. 1991; (3) Strom et al. 1989b.

referred to hereafter as "outflow sources," and sources that have no indication of CO outflow as "nonoutflow sources." Table 1 lists sources and their *IRAS* data.

Figure 1 shows the spatial distribution of 28 sources superposed on a contour map of ^{13}CO ($J = 1$–0) integrated intensity of L1641 (Fukui & Mizuno 1991). Most of the selected sources are associated with the molecular cloud. Using the data in Table 1, we can examine the far-infrared properties of the sources to make some preliminary classifications. The *IRAS* color-color diagram based on 12, 25, and 60 μm fluxes has often been used to classify different types of the sources, because various sources occupy different loci of the diagram (Beichman 1986; Emerson 1988; Fukui 1988; Fukui et al. 1989). In Figure 2 we plotted all the sources having detection in at least two of the three bands. It is evident in Figure 2 that most of the outflow sources are at the lower left and show relatively low color temperature. Sixteen of 28 sources are located inside the two boxes defined by Emerson (1988) as the locations of dense cores and T Tauri stars. Another five sources have optical counterparts or driving CO outflow. Thus, it is likely that most of the 28 sources are self-heated, although the several sources above the dense core box may include hot cirrus components.

2.2. *Millimeter Observations*

The radio observations were carried out in 1990 March and April by using the 45 m telescope of the Nobeyama Radio

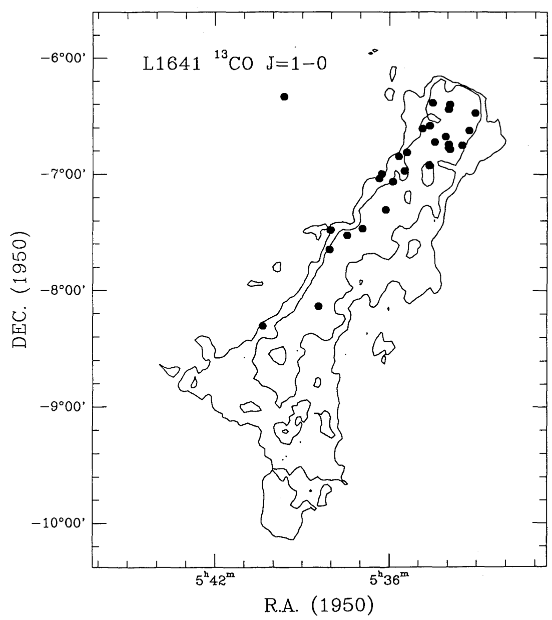

FIG. 1.—Spatial distribution of 28 *IRAS* sources in L1641 observed in this study. The two contours are the 3.0 and 7.0 K km s^{-1} integrated intensity of the ^{13}CO $J = 1$–0 emission (Fukui & Mizuno 1991).

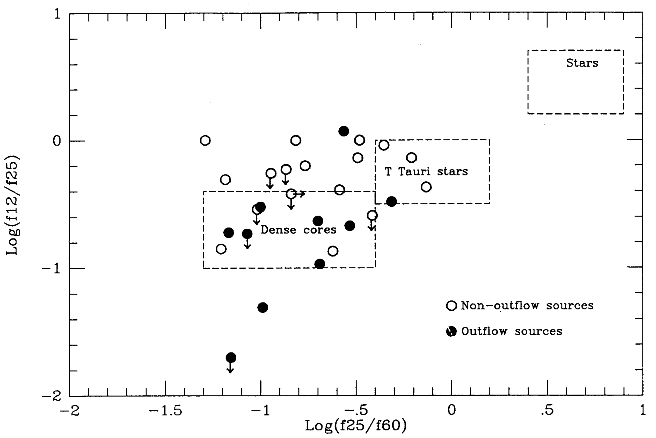

FIG. 2.—*IRAS* color-color diagram of 12, 25, and 60 μm fluxes. The boxes outline the specific locations of various *IRAS* sources (Emerson 1988). The filled circles are outflow sources, and the open ones are nonoutflow sources.

Observatory.[2] We observed each source in ^{13}CO ($J = 1$–0) and HCO$^+$ ($J = 1$–0) simultaneously. The observations consisted of two parts. For the first part, we made a five-point map centered on the *IRAS* position with an offset of 20″ in both R.A. and declination. For the second part, we made maps approximately 3′ × 3′ for three outflow sources (sources 8, 75, and 104) in a 20″ grid. The telescope beam sizes of 17″ and 20″ were used for ^{13}CO and HCO$^+$ transitions, respectively. A SIS receiver was used for the ^{13}CO line with a system temperature of 600 K in a single sideband at 110 GHz, and the HCO$^+$ line was observed using a cooled Schottky receiver with a system temperature of 800 K in a single sideband at 89 GHz at zenith. The 2048 channel acoustic-optical radio spectrometers yielded a spectral resolution of 250 kHz (or 0.65–0.85 km s^{-1}). The calibration for atmospheric and ohmic losses was made by the standard chopper wheel technique. We used position switching with the off positions about 1° from the sources. The intensity calibration was made by observing the standard source Ori A. For the pointing calibration, the telescope was pointed to the Ori A SiO maser source every 2–3 hr. The peak-to-peak pointing error was typically 7″.

To estimate the excitation temperature of ^{13}CO gas, the CO $J = 1$–0 line was also observed at each *IRAS* position using the 4 m telescope at Nagoya University. The beam size was 2.′7 at 115 GHz. A SIS receiver yielded a system temperature of 400 K in a single side band at zenith with frequency resolution of 50 KHz.

3. RESULTS

3.1. *Column Densities of the Molecular Gases*

The data obtained from both the Nobeyama and Nagoya observations were reduced using the Nagoya data reduction system. We made reliable detections of ^{13}CO emission in all 28 sources. The HCO$^+$ line was detected in 23 sources. In both the five-point maps and the 3′ × 3′ maps, we used the spectrum with the strongest emission line to calculate the line parameters. This gives us the line parameters corresponding to the emission peaks. Some sources have double peaks in both the ^{13}CO and HCO$^+$ profiles, showing multiple components in the line of sight. In such cases, the HCO$^+$ line was examined to select the strongest component. If two peaks were comparable in intensity, both of them were selected as sources a and b, respectively. Figure 3 displays the ^{13}CO and HCO$^+$ line profiles of source 216. A Gaussian fitting was carried out on each selected line to deduce the peak temperature T_p, the line width (FWHM) Δv, and the line center $V_{\rm LSR}$. These parameters are presented in Table 2. Using these data, we can derive the column densities of ^{13}CO and HCO$^+$ molecular gases.

Assuming (1) CO is optically thick and ^{13}CO is optically thin, and (2) the two transitions have the same excitation temperature, the column density of ^{13}CO can be calculated as follows:

$$N(^{13}{\rm CO}) = 2.49 \times 10^{14} \frac{T_{\rm ex}\, \tau_0^{13}\, \Delta v_{13}}{1 - \exp\,(-5.31/T_{\rm ex})}\,, \qquad (1)$$

where $T_{\rm ex}$ is the excitation temperature of ^{13}CO molecular gas that can be obtained using the above assumptions and Δv_{13} is the linewidth (FWHM) of ^{13}CO (Scoville et al. 1986). The optical depth at the ^{13}CO line peak, τ_0^{13}, can be obtained by using the observed peak temperatures of CO and ^{13}CO. Although the CO data were obtained using the 4 m telescope with a much larger beam, they can still be incorporated with the high-resolution ^{13}CO observations because the CO distribution is much more extended and uniform than the ^{13}CO gas distribution.

If the HCO$^+$ $J = 1$–0 line is optically thin, the HCO$^+$ column density can be written as

$$N({\rm HCO}^+) = 1.87 \times 10^{11} \frac{T_{\rm ex}\, T_p\, \Delta v}{1 - \exp\,(-4.3/T_{\rm ex})}\,, \qquad (2)$$

where T_p and Δv are the peak temperature and FWHM of the HCO$^+$ line, respectively (Yang et al. 1991). The HCO$^+$ excitation temperature $T_{\rm ex}$ is more difficult to determine, and it is likely different from the CO excitation temperature. Fortunatey, the HCO$^+$ column density is not very sensitive to the excitation temperature. Using the LVG model (Goldreich & Kwan 1974), we found that for the $T_{\rm ex} = 10$–20 K, the calculated column density changes only by a factor of 2. We therefore assume a constant $T_{\rm ex} = 15$ K. The column densities of

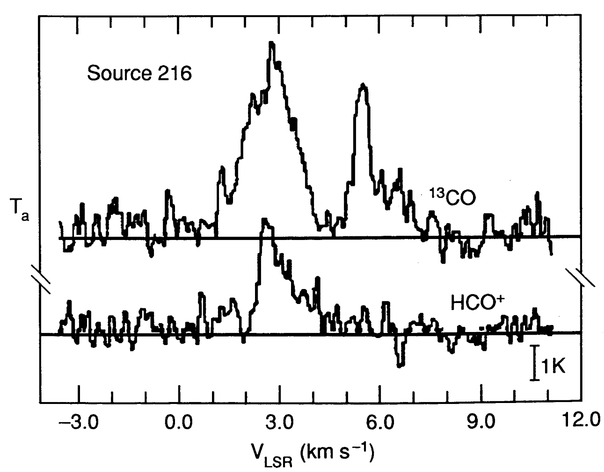

FIG. 3.—Line spectra taken at the position of source 216 (L1641-S2). The top line is ^{13}CO ($J = 1$–0), and the bottom one is HCO$^+$ ($J = 1$–0). Note that only the component at 3.0 km s^{-1} was used.

[2] The Nobeyama Radio Observatory is a branch of the National Astronomical Observatory, an inter-university research institute operated by the Ministry of Education, Science, and Culture, Japan.

TABLE 2

Millimeter Line Parameters and Column Densities

Number	^{13}CO T_p (K)	T_{rms} (K)	Δv (km s^{-1})	V_{LSR} (km s^{-1})	CO T_p (K)	HCO$^+$ T_p (K)	T_{rms} (K)	Δv (km s^{-1})	V_{LSR} (km s^{-1})	τ_0^{13}	$N(^{13}CO)$ (10^{15} cm^{-2})	$N(HCO^+)$ (10^{12} cm^{-2})
3	3.6	0.44	0.7	7.4	16.8	0.8	0.24	0.3	7.7	0.24	2.5	2.5
7	4.5	0.55	1.6	8.8	13.2	...	0.33	...	...	0.42	6.6	<6.7
8	7.4	0.57	2.9	6.7	25.7	3.1	0.31	1.9	6.9	0.34	33.5	67.7
18	7.0	0.37	2.2	6.1	20.8	1.1	0.23	2.0	7.2	0.41	20.6	24.1
25	7.1	0.57	2.0	8.2	24.6	4.0	0.48	1.0	8.8	0.34	21.7	43.7
31	3.5	0.50	1.9	6.9	17.6	0.7	0.16	0.9	7.0	0.22	7.2	7.0
33a	2.5	0.72	1.5	9.1	13.6	...	0.25	...	...	0.20	3.1	<3.9
33b	1.9	0.72	2.2	6.3	13.6	...	0.25	...	...	0.15	3.5	<3.9
34a	4.5	0.47	0.8	8.1	21.9	1.0	0.28	1.0	8.8	0.23	4.5	11.0
34b	3.2	0.47	1.3	7.1	21.9	0.8	0.28	0.5	7.4	0.16	5.2	4.9
37a	5.5	0.41	0.8	8.3	16.5	0.9	0.30	1.5	9.0	0.41	4.7	15.6
37b	4.7	0.41	1.0	6.3	16.5	1.2	0.30	0.7	6.9	0.34	5.1	10.0
42	3.6	0.28	1.3	6.5	20.4	0.7	0.22	0.5	6.9	0.19	5.8	4.0
47	7.7	0.55	1.4	8.2	25.1	0.9	0.32	1.2	9.1	0.37	16.7	12.6
49	4.7	0.35	1.4	6.3	27.1	1.7	0.29	0.5	6.3	0.19	10.0	9.8
50	8.1	0.39	2.0	8.1	26.2	1.8	0.17	1.5	8.7	0.37	26.4	31.0
51	8.7	0.56	3.4	8.0	25.5	2.0	0.34	2.1	9.1	0.42	47.9	46.8
56	3.5	0.44	2.0	5.7	13.7	1.3	0.19	1.0	5.7	0.30	6.2	14.8
62	2.8	0.68	3.1	6.4	13.8	...	0.25	...	...	0.23	7.6	<4.6
68	3.3	0.79	1.0	8.5	16.6	0.8	0.23	0.6	8.5	0.22	3.2	4.6
71	5.3	0.39	1.6	4.8	17.7	0.9	0.16	0.9	5.8	0.36	9.9	9.2
73	4.7	0.80	2.5	3.3	14.3	...	0.41	...	...	0.40	11.3	<6.7
75	5.1	0.50	3.1	2.3	13.3	2.2	0.29	1.0	3.1	0.48	15.1	23.8
79	4.7	0.35	1.5	4.8	14.4	0.9	0.27	1.5	5.4	0.40	7.0	15.0
96	3.9	0.59	1.7	6.2	14.2	0.7	0.20	0.7	6.6	0.32	6.2	5.1
104	5.0	0.50	2.0	3.9	11.6	1.8	0.36	2.2	3.6	0.56	9.0	44.8
105	4.5	0.44	3.9	4.1	10.1	1.1	0.31	1.2	5.5	0.59	14.0	14.2
108	3.9	0.50	2.7	4.8	13.5	...	0.45	...	...	0.34	9.6	<7.3
119	4.9	0.62	2.0	4.5	11.3	...	0.30	...	...	0.57	8.4	<5.0
194	3.4	0.82	1.5	5.1	13.5	1.7	0.61	1.4	5.2	0.29	4.5	26.4
216	4.8	0.51	1.6	3.0	13.0	2.7	0.33	1.2	3.1	0.46	7.3	35.6

^{13}CO and HCO$^+$ calculated from equations (1) and (2) are listed in Table 2 as $N(^{13}CO)$ and $N(HCO^+)$, respectively.

3.2. *Correlation Studies*

Figure 4 is a diagram of the ^{13}CO and HCO$^+$ column densities. There is a clear correlation between the two column densities. Sources that have large $N(HCO^+)$ also have large $N(^{13}CO)$. In Figures 5*a* and 5*b*, we plotted the *IRAS* colors defined by the ratio of the *IRAS* fluxes at 12–25 μm against the $N(^{13}CO)$ and $N(HCO^+)$, respectively. Figure 5 clearly shows the correlations between the gas column densities and the *IRAS* color. The cold *IRAS* sources (smaller $f12/f25$) tend to be associated with higher gas column densities. This trend is clearer for HCO$^+$ than for ^{13}CO, as suggested by the correlation coefficients of the two diagrams, 0.79 and 0.68, for Figures 5*a* and 5*b*, respectively. While the physical implications of these correlations will be discussed in § 4, the correlations suggest that the line emissions we detected come from the gases associated with the *IRAS* sources, and that they are not foreground or background emission.

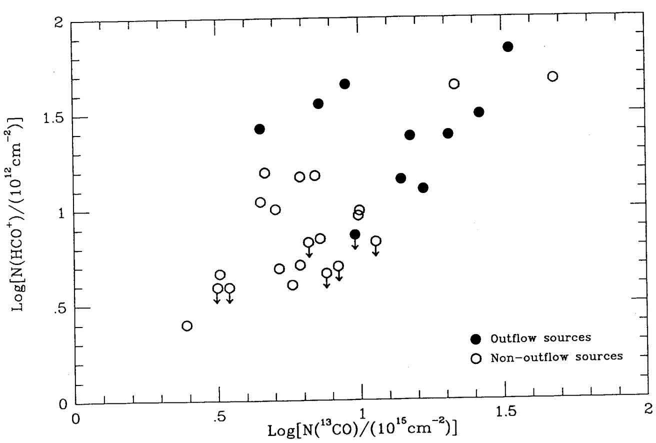

Fig. 4.—Comparison of the ^{13}CO and HCO$^+$ column densities. The filled circles are the outflow sources, and the open ones are nonoutflow sources. Arrows indicate 3 σ upper limits.

3.3. *Maps of Three Outflow Sources*

Figure 6 presents the contour maps of the HCO$^+$ integrated intensity for three outflow sources. In all three maps, the lowest contour represents the 40% level of the maximum integrated intensity for each source and the contour interval is about 3 σ. In each field, there is a well-defined core located close to the *IRAS* sources position, as indicated by the crosses.

The high-resolution mapping enables us to characterize the HCO$^+$ dense cores. We used the minimum and maximum sizes of the half-maximum contour and took a geometrical average of them to derive radius R. Two of the three cores (sources 8 and 104) are larger than the 20″ beam size and do not show structure within the cores. Since the core near source 75 shows 2–3 components, only the main component (SW of the *IRAS* position) was calculated. The number density of molecular gas can then be estimated by assuming a uniform core density and

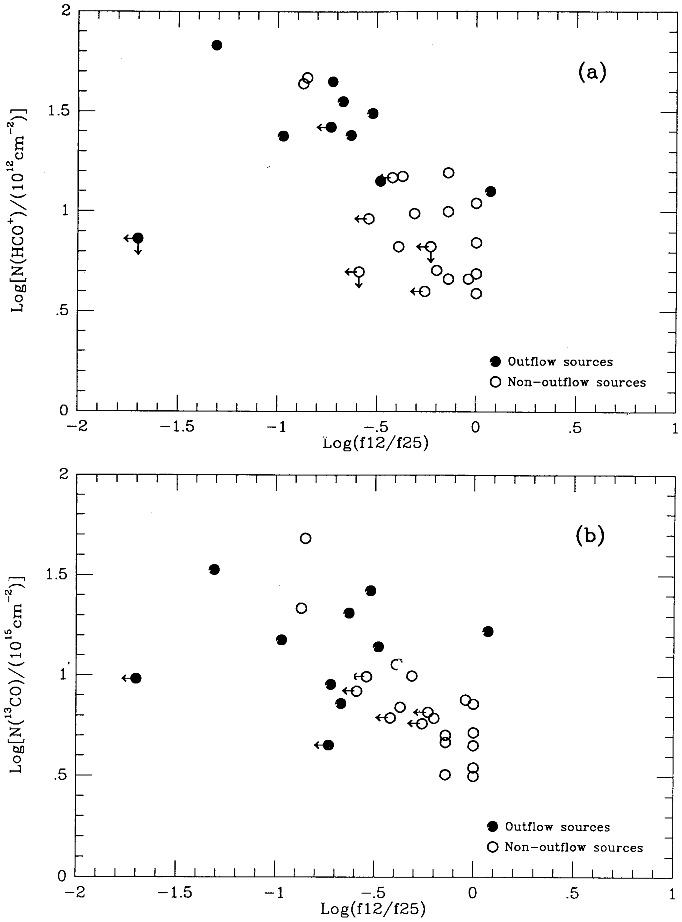

FIG. 5.—Column density vs. *IRAS* color defined by 12 to 25 μm flux ratio for (*a*) HCO^+ column density and (*b*) ^{13}CO. Downward arrows indicate 3 σ HCO^+ upper limits. The leftward arrows indicate 5 σ 12 μm upper limits. Sources with no detections at 12 and 25 μm are not plotted.

HCO^+ abundance. The latter may vary from source to source, depending on kinetic temperature and density of the gases. For the first-order analysis in this study, we adopted $X(HCO^+) = 10^{-9}$ derived by Wotten, Snell, & Evans (1980) for three dark clouds with $T_k < 20$ K, although it might be too high for L1641-North. The physical parameters of the three cores are summarized in Table 3. We now discuss each source in turn.

Source 8 (L1641-North) is one of the brightest and coldest *IRAS* sources in L1641. It is associated with L1641-North, the most powerful outflow in L1641 (Fukui et al. 1986; Wilking, Blackwell, & Mundy 1990). The near-IR imaging shows a young cluster associated with the *IRAS* source (Strom, Margulis, & Strom 1989a; Chen, Tokunaga, & Hodapp 1992d). The contour map (Fig. 6*a*) shows a structure similar to that seen by Fukui et al. (1988) in their HCO^+ observations. The core is elongated at 45° northeast, along the same direction as the CO outflow. It is interesting that our high-resolution ^{13}CO contour map shows no well-defined core within the 2′–3′ field. Considering that the low-resolution mapping does show a well-peaked ^{13}CO core (Chen, Fukui, & Itawa 1992b), we argue that the ^{13}CO core has a size greater than 3′, which is at least 6 times larger than the HCO^+ core. Such a large structure of 7′–8′ was in fact mapped in the ^{13}CO emission by Takaba et al. (1986).

The CO outflow (L1641-Center) associated with source 75 was first identified and mapped with the Nagoya 4 m telescope by Takaba (1986). The blue high-velocity wing is dominant, while the red wing is weaker. This outflow is extended over 6′ as mapped with the Nagoya 4 m telescope (Fukui et al. 1992). The recent CO $J = 2$–1 and 3–2 observations also confirmed the existence of the outflow (Sugitani et al. 1992). Morgan et al. (1991), however, argue that the high-velocity wing is due to the multiple velocity components, not the outflow from the embedded source. We suggest that the area mapped by Morgan et al. (1991), 6′ × 6′, was not large enough to localize the high-velocity emission. The high-resolution map of this study allows us to explore the central region of the dense gas in much more detail. As shown in Figure 6*b*, within the field of 2′ × 2′, we detected two molecular condensations. The main clump is located 60″ W and 40″ S of the *IRAS* position. There is also a weaker clump to the east. The near-IR imaging (Chen et al. 1992a) shows signs of young stellar clustering near the *IRAS* position. One source showing bipolar nebulosity is located very close to the main clump, while another very red source (detectable only at 3.6 μm) is near the *IRAS* position. The high-resolution map and the IR images suggest multiple YSOs near source 75. Further high spatial and spectral resolution interferometer observations are clearly needed.

Source 104 has been identified as emission-line star Haro 4-255. There is another far-infrared source (Haro 4-255 FIR) located about 1′ to the northwest of Haro 4-255 (Evans, Leverault, & Harvey 1986; Leverault 1988). Both sources are marked on the HCO^+ map in Figure 6*c*. Although the two sources seem to have different color temperatures at 50–100 μm, it is not clear whether they are the same source or two different sources, because the far-infrared emission may well be contaminated by the other source. Our integrated intensity map shows a well-defined core; however, the position-velocity map (Fig. 7) clearly shows two velocity components separated by 2 km s^{-1}. The major component is close to the *IRAS* position, and the secondary component is close to Haro 4-255-FIR. A recent CS emission line survey of L1641 also indicated two components in this region (Tatematsu & Umemoto 1991). In Figure 7, the velocity structure of the main component is much more extended than that of the secondary, showing signs of a high-velocity wing. We therefore suggest that both Haro 4-255 and Haro 4-255 FIR are associated with molecular dense gas.

TABLE 3

PHYSICAL PARAMETERS OF THREE HCO^+ CORES

Number	ID	$N(HCO^+)$ (10^{13} cm^{-2})	Δv (km s^{-1})	R (pc)	$n(H_2)$ (10^5 cm^{-3})	M ($M_\odot$)
8.........	L1641-North	6.8	1.94	0.16	1.4	27
75.........	L1641-Center	2.4	0.96	0.09	0.9	3
104.........	H4-255	4.5	2.21	0.11	1.4	8

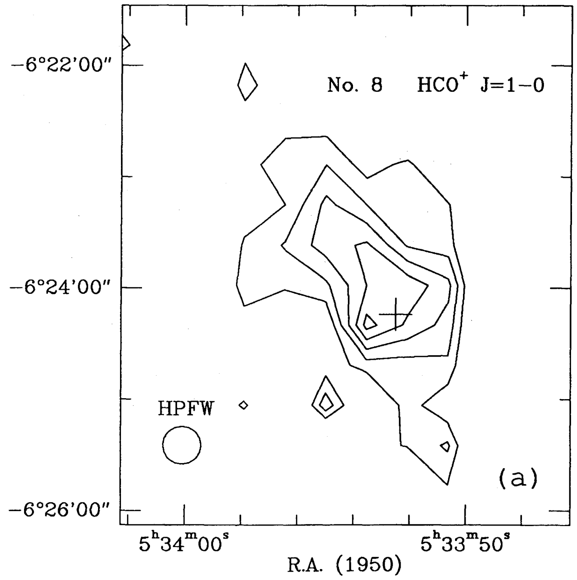

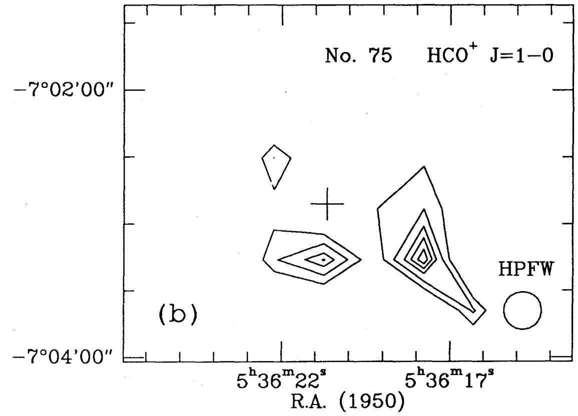

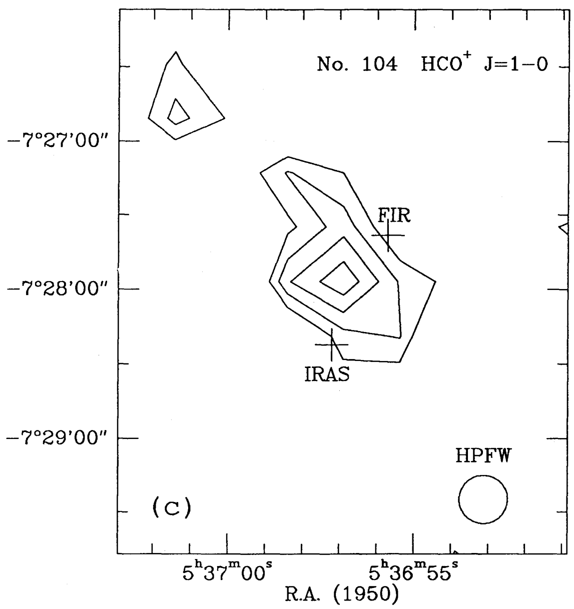

FIG. 6.—Contour maps of HCO^+ integrated intensity of three outflow sources. The lowest contour represents 40% of maximum, and the interval is about 3 σ. (*a*) Source 8 (L1641-North); (*b*) source 75 (L1641-Center); (*c*) source 104 (H4-255). The *IRAS* source positions are marked by the crosses.

The core in which Haro 4-255 is embedded has more extended velocity structure and is probably the driving source of the CO outflow.

4. DISCUSSION

In § 3, the following three results were obtained from the present observational data: (1) there is a correlation between the ^{13}CO column density and HCO^+ column density; (2) the molecular column densities are well correlated with the infrared color of the *IRAS* sources defined as log ($f12/f25$) (outflow sources tend to have higher column densities and smaller flux ratio, or lower color temperature); and (3) all three outflow sources we mapped are associated with well-defined HCO^+ cores with masses of 3–30 $M_\odot$, assuming a HCO^+/H_2 of 10^{-9}. We now discuss the implications of these results below.

4.1. *The Association of the Dense Cores with Outflow Sources*

The correlation of molecular column densities with the *IRAS* color suggests the gases probed by our observations are associated with the *IRAS* sources, and they are not foreground or background gases. For the three outflow sources mapped, we found well-defined dense cores near the *IRAS* source positions. The outflow sources also tend to have higher column density than the nonoutflow sources. In Table 2, 9 of 10 outflow sources have $N(HCO^+)$ higher than 1.2×10^{13} cm^{-2}, while 14 of 18 nonoutflow sources have $N(HCO^+)$ lower than that value. We conclude that most outflow sources are associated with molecular dense cores, and most nonoutflow sources are probably not associated with a dynamically stable dense core.

4.2. *Core Dissipation During Star Formation*

There are two explanations why outflow sources tend to be associated with dense cores and nonoutflow sources do not: (1) proper motion of the YSOs with respect to the dense cores in

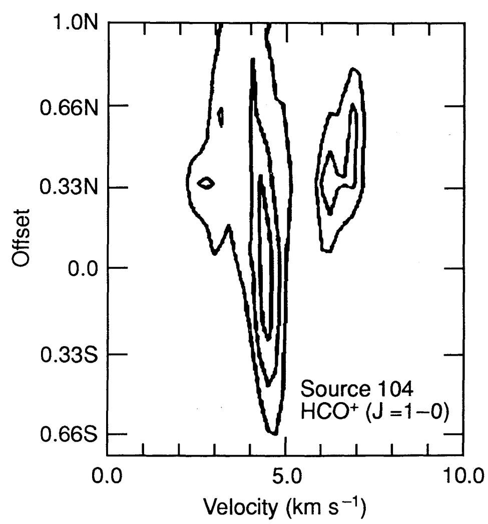

FIG. 7.—Velocity-position diagram of source 104. The north-south cut was made at the *IRAS* position.

which they were born, and (2) core dissipation by accretion and outflow of the central embedded sources.

If a young star is first formed at the center of a molecular dense core and moves away from the core when it becomes a T Tauri-type star, we can calculate the star's velocity dispersion with respect to its associated molecular gas:

$$\Delta V = 1.0 \left(\frac{R_{\rm core}}{\rm pc}\right)\left(\frac{10^6 \ {\rm yr}}{T_{\rm TTS}}\right) \ {\rm km \ s^{-1}} , \qquad (6)$$

where $R_{\rm core}$ is the radius of the core (0.1 pc for HCO^+ cores and 1–2 pc for ^{13}CO cores). Taking the average age of T Tauri stars to be 10^6 yr (Cohen & Kuhi 1979), a velocity dispersion of 0.1 km s^{-1} or 1.0–2.0 km s^{-1} is required for a YSO to move away from its HCO^+ core or ^{13}CO core, respectively. The observations of the proper motion of the T Tauri stars with respect to their associated molecular gas yielded only upper limits. The most recent observations in Taurus-Auriga and the Orion Complex (Hartmann et al. 1986) found the velocity dispersion less than 1.5 km s^{-1}. Such a dispersion is probably not enough for YSOs to escape the ^{13}CO cores, although it remains uncertain whether the proper motion is large enough for YSOs to escape their HCO^+ cores.

The other possibility is core dissipation during the early evolution of the star. Two mechanisms can cause such dissipation: (1) accretion by which a protostar builds up its mass, and (2) enormous mass loss by the YSO as detected by CO line emission. The dissipation may be accomplished when the protostars become the T Tauri-type stars. For a dense core of 3 $M_\odot$, and assuming the age of T Tauri stars to be 10^6 yr, a dissipation rate of 3×10^{-6} $M_\odot$ yr^{-1} is necessary if the core can be dissipated when the central star becomes T Tauri-type star. Because it is comparable with the accretion rate (10^{-5} $M_\odot$ yr^{-1}) and the mass-loss rate of the CO outflow (2×10^{-6} $M_\odot$ yr^{-1}) within the uncertainties, we suggest that the both accretion and outflow can dissipate the molecular cores. If star formation takes place in a cluster, such as in L1641-North, the dissipation of a more massive core (10–100 $M_\odot$) by accretion and outflow will be feasible.

4.3. *Indicators of Evolutionary State of the IRAS Sources*

We studied the *IRAS* source emission in three different spatial scales: (1) far-infrared emission at a scale of 10^{15-16} cm (the radiative equilibrium radius); (2) high-excitation HCO^+ line emission at 10^{16-17} cm, and (3) the low-excitation ^{13}CO line emission at 10^{17-18} cm. The *IRAS* color log (($f12/f25$), the HCO^+ column density, and the ^{13}CO column density each probes different regions near the YSO. The correlations discussed in § 3 show that they could be governed by the same physical process. Although the ^{13}CO line emission suffers contamination from foreground and background gas, it can still be used to indicate the evolutionary state of the YSOs. The much improved correlation between HCO^+ column density and *IRAS* 12–25 μm flux ratio in Figure 5*a* shows that $N(HCO^+)$ is a better indicator of the evolutionary state of the YSOs. This is no surprise because the HCO^+ emission comes from a very compact region near the sources and the 12–25 μm ratio measures the color temperature of the dust closest to the sources.

While further detailed studies are needed, we propose the following scenario to reconcile the results obtained in this study. If the *IRAS* emission comes from the dust heated by the central embedded sources, the *IRAS* flux ratio is a measure of the color temperature of the dust. In the early stage of protostar formation, the dust shell is so thick that high-frequency photons are degraded into the low-frequency photons. These sources should appear to be cold as observed by *IRAS* observations. Meanwhile, since the sources are still deeply embedded, the ^{13}CO and HCO^+ column densities toward the *IRAS* sources should measure the dense gas of the dense core in which the protostars are embedded. When the protostar starts to build up its mass by accretion, an outflow develops at the center that dissipates the dust structure, both the inner dense core as measured by HCO^+, and the outer structure as measured by ^{13}CO. Because of the observed correlations (see Figs. 4 and 5), such dissipation occurs concentrically around the YSO at comparable rates.

5. SUMMARY

To understand the relationship between YSOs and their environment, we have undertaken high-resolution ^{13}CO (J = 1–0) and HCO^+ (J = 1–0) observations of 28 *IRAS* sources selected from the *IRAS* co-added images. All sources have ^{13}CO emission, and 23 sources have HCO^+ emission. Three outflow sources are fully mapped. The main results are summarized as follows:

1. All three mapped outflow sources are associated with the well-defined HCO^+ cores near the *IRAS* source position. The average size of the cores is about 0.1 pc with a mass of 3–30 $M_\odot$.
2. There is a strong correlation between the ^{13}CO and HCO^+ column densities. Both column densities are also correlated with the *IRAS* color defined by the flux ratio at 12 and 25 μm.
3. Based on the above results, we conclude that the outflow sources are associated with molecular dense cores and that of the nonoutflow sources are not associated with a dense core. Such a difference is probably caused by dissipation of the dense cores during the star-formation process. Both accretion and the CO outflow are capable of dissipating the cores.
4. The above correlations show that the column densities of ^{13}CO and HCO^+ and the *IRAS* 12–25 μm flux ratio could be indicators of the evolutionary states of the YSOs, although the HCO^+ column density and the *IRAS* color give more accurate results.

We like to thank A. T. Tokunaga for many helpful discussions. It is our pleasure to thank the staff at IPAC for providing us with the *IRAS* co-added images and addscan data. We also thank the staff at Nobeyama Radio Observatory for making the observations possible. H. C. was supported in part by a fieldwork fellowship from the East West Center, USA. This research was also supported in part by the Grant-in-Aid for specially supported research No. 01065002 and the Monbusho International Scientific Research Program: Joint Research No. 02044064 of the Ministry of Education, Science and Culture, Japan.

REFERENCES

Bally, J., Langer, W. D., Stark, A. A., & Wilson, R. W. 1987, ApJ, 312, L45
Beichman, C. A. 1986, in Light on Dark Matter, ed. F. P. Israel (Dordrecht: Reidel), 279
Beichman, C. A., Myers, P. C., Emerson, J. P., Harris, S., Mathieu, R., Benson, P. J., & Jennings, R. E. 1986, ApJ, 307, 337
Chen, H., et al. 1992a, in preparation
Chen, H., Fukui, Y., & Iwata, T. 1992b, in preparation
Chen, H., Tokunaga, A. T., & Fukui, Y. 1992c, in preparation
Chen, H., Tokunaga, A. T., & Hodapp, K.-W. 1992d, in Proc. Vulcano Workshop on Young Star Clusters and Early Stellar Evolution, ed. F. Palla & H. Zinnecker, in press
Cohen, M., & Kuhi, L. O. 1979, ApJS, 41, 743
Emerson, J. P. 1988, in Formation and Evolution of Low-Mass Stars, ed. A. P. Dupree & M. T. V. I. Lago (Dordrecht: Kluwer), 193
Evans II, N. J., Leverault, R. M., & Harvey, P. M. 1986, ApJ, 301, 894
Fukui, Y. 1988, Vistas Astron., 31, 217
———. 1989, in Proc. ESO Workshop on Low-Mass Star Formation and Pre–Main-Sequence Objects, ed. B. Reipurth (Garching: ESO), 95
Fukui, Y., et al. 1992, in preparation
Fukui, Y., Iwata, T., Takaba, H., Mizuno, A., Ogawa, H., Kawabata, K., & Sugitani, K. 1989, Nature, 342, 161
Fukui, Y., & Mizuno, A. 1991, in IAU Symp. 147, Fragmentation of Molecular Clouds and Star Formation, ed. E. Falgarone, F. Boulanger, & G. Duvert (Dordrecht: Kluwer), 275
Fukui, Y., Sugitani, K., Takaba, H., Iwata, T., Mizuno, A., Ogawa, H., & Kawabata, K. 1986, ApJ, 311, L85
Fukui, Y., Takaba, H., Iwata, T., & Mizuno, A. 1988, ApJ, 325, L13
Goldreich, P., & Kwan, J. 1974, ApJ, 189, 441
Hartmann, L., Hewett, R., Stahler, S., & Mattieu, R. D. 1986, ApJ, 309, 275
Herbig, G. H., & Bell, K. R. 1988, Lick Obs. Bulletin No. 1111
IRAS Point Source Catalog, Version 2 1988, Joint *IRAS* Science Working Group (Washington, DC: GPO) (PSC)
Leverault, R. M. 1988, ApJS, 67, 283
Morgan, J., Schloerb, F. P., Snell, R. L., & Bally, J. 1991, ApJ, 376, 618
Myers, P. C., & Benson, P. J. 1983, ApJ, 266, 309
Scoville, N. Z., Sargent, A. I., Sanders, D. B., Clauseen, M. J., Masson, C. R., Lo., K. Y., & Philips, T. G. 1986, ApJ, 303, 416
Strom, K. M., Margulis, M., & Strom, S. E. 1989a, ApJ, 346, L33
Strom, K. M., Newton, G., Strom, S. E., Seaman, R. L., Carrasco, L., Cruz-Gonzalez, I., Serrano, A., & Grasdalen, G. 1989b, ApJS, 71, 183
Shu, F., Adams, F., & Lizano, S., 1987, ARA&A, 25, 23
Sugitani, K., et al. 1992, in preparation
Takaba, H. 1986, Ph.D. thesis, Nagoya Univ.
Takaba, H., Fukui, Y., Fujimoto, Y., Sugitani, K., Ogawa, H., & Kawabata, K. 1986, A&A, 166, 276
Tatematsu, K., & Umemoto, T. 1991, private communication
Wilking, B. A., Blackwell, J. H., & Mundy, L. G. 1990, AJ, 100, 758
Wotten, A., Snell, R., & Evans II, N. J. 1980, ApJ, 240, 532
Yang, J., Umemoto, T., Iwata, T., & Fukui, Y. 1991, ApJ, 373, 137